

# Deep Learning-Optimized Dielectric Laser Accelerators: High-Gradient Performance and Cascaded Photonic Chip

Peng-Bo Chen,<sup>1</sup> Shao-Yi Wang,<sup>2</sup> Wen-Bo Zhang,<sup>3</sup> Rong-Wei Zha,<sup>1</sup> Bin Sun,<sup>4</sup> Jia-Xing Wen,<sup>2</sup> Cheng Lei,<sup>1,\*</sup> Zong-Qing Zhao,<sup>2,†</sup> and Du Wang<sup>1,‡</sup>

<sup>1</sup>The Institute of Technological Sciences, Wuhan University, Wuhan 430072, China

<sup>2</sup>National Key Laboratory of Plasma Physics, Laser Fusion Research Center, CAEP, Mianyang 621900, China

<sup>3</sup>School of Civil Engineering, Wuhan University, Wuhan 430072, China

<sup>4</sup>School of Physics and Astronomy, China West Normal University, Nanchong 637009, People's Republic of China

Dielectric laser accelerators (DLAs) can achieve acceleration gradients exceeding those of conventional radio-frequency accelerators by one to two orders of magnitude. Existing DLA design approaches rely heavily on empirical parameter tuning and single-variable optimization, which fundamentally constrains performance enhancement. Here, a new optimization strategy for DLA structures is proposed based on the Gated Adaptive Network for Deep Automated Learning of Features (GANDALF). This framework integrates key parameters such as geometric configurations, material properties, and optical field characteristics into a comprehensive analysis. By accurately predicting particle energy gain, the structural parameters are optimized, significantly improving DLA performance. The proposed approach outperforms traditional computational methods, particularly for nonperiodic structures, enabling continuous particle acceleration. The GANDALF model demonstrates high accuracy, robustness, and adaptability, yielding an average acceleration gradient of 2.8 GV/m ( $\text{Y}_2\text{O}_3$ ), enabling sustained acceleration in the majority of the acceleration channel, with a beam spot radius of 3.13  $\mu\text{m}$ . Additionally, a cascaded DLA design concept is introduced and validated, paving the way for extended acceleration lengths on photonic chips.

Keywords: Dielectric laser accelerators, Deep learning, GANDALF, Cascaded design, Nonperiodic structures

## I. Introduction

Accelerators play a pivotal role in a wide range of fields, including fundamental physics experiments, materials characterization, cancer treatment, and medical diagnostics [1–3]. Traditional microwave-based accelerators, while well-established, suffer from limitations such as large physical footprint and low acceleration gradients, making them less suitable for compact and cost-effective applications [4, 5]. This has driven the search for alternative technologies, with dielectric laser accelerators (DLAs) emerging as a highly promising solution. DLAs, have attracted significant attention owing to their optical-scale compactness and efficient energy conversion capabilities, have gained significant attention [6]. In the 1980s, the inverse Smith–Purcell effect was demonstrated using terahertz radiation and metallic gratings, albeit with relatively low acceleration gradients (of the order of keV/m) [7]. Modern dielectric materials, such as silica, exhibit damage thresholds of up to 1 GV/m, theoretically enabling DLAs to achieve acceleration gradients on the order of GV/m [8, 9]. Experimental results demonstrate that current DLAs can already achieve gradients approaching 1 GV/m [10–12]. Among the various DLA designs, there are three primary optical configurations: photonic crystal fibers [15], stacked structures [16], and grating structures [17–19]. Grating structures are particularly attractive due to their simple geometry and relatively uniform optical field distribution, making them easier to analyze and integrate into chip-based

designs [20]. Consequently, much of the research on DLA optimization has focused on grating structures, as their material and geometric parameters directly influence the electric field distribution in the acceleration region, thereby affecting the motion of the particle beam [21, 22]. Accordingly, considerable research effort has been directed toward the geometric and topological optimization of DLA photonic crystals [21, 23]. Existing DLA design methods primarily rely on empirical tuning of parameters and single-variable optimization, which limits both efficiency and adaptability. These methods also tend to lack generalizability and cannot easily accommodate complex experimental requirements. Moreover, most designs to date have been limited to periodic grating structures, which inevitably introduce deceleration phases as acceleration distances increase. To date, no effective optimization method for nonperiodic DLA structures has been reported. With the rapid development of artificial intelligence, deep learning has shown considerable promise in the design of photonic and optoelectronic devices [24–30]. Unlike traditional design methods, deep learning enables the extraction of complex patterns from multidimensional data, allowing for the precise identification of key structural parameters while minimizing computational costs. For instance, Hughes et al. [21] used topology optimization methods for DLA structures, but many deep learning approaches still rely on static, single-field images, which are insufficient to fully capture the effects physics governing particle acceleration. The potential for deep learning to address these shortcomings, particularly in nonperiodic designs, remains largely untapped. Additionally, the intrinsic properties of dielectric laser accelerators facilitate their integration onto chip platforms [31], thereby enhancing particle beam energy gain while maintaining beam quality. This is particularly advantageous in the context of

\* Corresponding author, Cheng Lei, leicheng@whu.edu.cn

† Corresponding author, Zong-Qing Zhao, zhaozongqing99@caep.ac.cn

‡ Corresponding author, Du Wang, wangdu@whu.edu.cn

cascaded acceleration designs, which present a promising avenue for further development [32].

This work presents, to the best of the authors' knowledge, the first deep learning-based design methodology for dielectric grating accelerators that optimizes nonperiodic photonic crystal structures. A comprehensive feature evaluation framework is established, incorporating geometric parameters, material properties, and optical field energy. Distinctively, the method combines geometric parameters and the target particle beam quality into a one-dimensional tabular dataset. The GANDALF model, which excels at processing non-sequential tabular data, is utilized as the deep learning framework. The model accurately predicts the target particle energy gain index and selects the parameters corresponding to the maximum energy gain, thereby optimizing the dielectric grating accelerator structure. The designed grating accelerator addresses the challenges of nonperiodic structure design, as well as the problems of decelerating phases in periodic structures and limitations in extending the acceleration distance in grating accelerators. Additionally, the average particle acceleration gradient reaches 2.8 GV/m, enabling sustained acceleration in the majority of the channel, with a beam spot radius of 3.13  $\mu\text{m}$ . Furthermore, extending this method to cascaded DLA designs validates the feasibility of long acceleration distances. This establishes a potential technological pathway for the design and development of high net-energy-gain particle accelerators based on photonic chips.

## II. METHODS

### A. Design Concept

In periodic grating structures, as the particle velocity increases during acceleration, the fixed spatial periodicity of the grating disrupts phase synchronization with the incident laser wavefront, owing to the uniform variation of the optical field across the entire structure. This results in deceleration in certain regions. To overcome this inherent limitation, modular structures with additional control parameters are introduced, offering the potential for sustained acceleration in localized regions. To achieve this, the acceleration region is modularized to control the wavefront phase in different regions, aiming for continuous phase matching between the particle velocity and the incident laser wavefront, which enables sustained acceleration. Achieving this goal relies on the use of complex, parameterized nonperiodic grating structures. Therefore, this study focuses on the exploration of nonperiodic grating structures as the primary research subject. The accelerator structure is illustrated in Figure 1(a), where the particle acceleration channel is centrally positioned within the device. Dielectric pillars are symmetrically arranged on either side of the acceleration channel, with pairs of dielectric pillars treated as a unit. As shown in Figure 1(b), each group of dielectric pillars is characterized by the parameter array  $\mathbf{D}_i = [l_i, w_i, \theta_i]$ , with each parameter exhibiting relative independence and minimal correlation in terms of geometric dimensions and spatial distributions. In addition to the size and distribution of the dielectric pillars, the refrac-

tive index of the dielectric material significantly impacts the acceleration performance of the grating accelerator.

The principle of sustained acceleration in the grating accelerator is depicted in Figure 1. The propagation speed of the laser pulse within the dielectric pillars is lower than that in the adjacent vacuum regions. This difference creates a phase shift of the electric fields in two neighboring regions of the particle acceleration channel. By adjusting the geometric characteristics of the dielectric pillars to induce a  $\pi$  phase difference in the electric field distribution between adjacent regions, continuous accelerating forces can be applied to the particles. The accelerator designed in this study enables each group of dielectric pillars to function as independent units by adjusting the parameter array  $\mathbf{D}_i = [l_i, w_i, \theta_i]$ . Particle acceleration across multiple regions is achieved by designing modular dielectric pillars whose electric field distributions are aligned with the local particle velocity. If particles can be accelerated across a larger portion of the structure, the resulting increase in particle energy will increase accordingly. Given the complexity of optical field variation in nonperiodic structures and the difficulty of capturing the underlying physical principles, the problem is simplified by treating more efficient particle energy gain as equivalent to accelerating particles across a larger fraction of the structure. On this basis, particle energy gain is selected as the primary figure of merit for this study. However, the increased complexity of this highly tunable grating structure presents challenges traditional numerical computational methods are time-consuming and heavily reliant on empirical data, making them less suitable for optimizing the nonperiodic grating structures.

### B. Deep Learning Method Based on the GANDALF Model

In this work, the GANDALF model is employed as the primary analytical tool. It is distinguished by its efficacy in processing high-dimensional data and nonlinear relationships. The model employs advanced feature learning techniques to optimize feature representation, significantly enhancing generalization capability and predictive accuracy. Furthermore, the GANDALF model's flexibility enables it to accommodate different data distributions and noise levels, enhancing its capacity for analyzing complex systems. In this study, the numerous feature parameters exhibit low mutual correlations, necessitating a deep learning model that can effectively handle complex feature information. Therefore, the application of the GANDALF model is expected to yield reliable results.

The deep learning methodology based on the GANDALF model is illustrated in Figure 2. This method comprises two steps. The first step involves establishing the database. The accelerator model is first constructed (Figure 2(a)), using a uniform laser wavelength of 1550 nm for plane-wave illumination, with a particle injection energy of 500 keV. The model dimensions are  $L = 6.26 \mu\text{m}$  and  $W = 6.2 \mu\text{m}$ . The design parameters for each group of dielectric pillars are denoted by the parameter array  $\mathbf{D}_i = [l_i, w_i, \theta_i]$ .

Next, optimal parameter ranges are established; three parameters are sampled independently, initially filtered through manual screening and subsequently refined through numerical simulation to determine the optimal ranges:

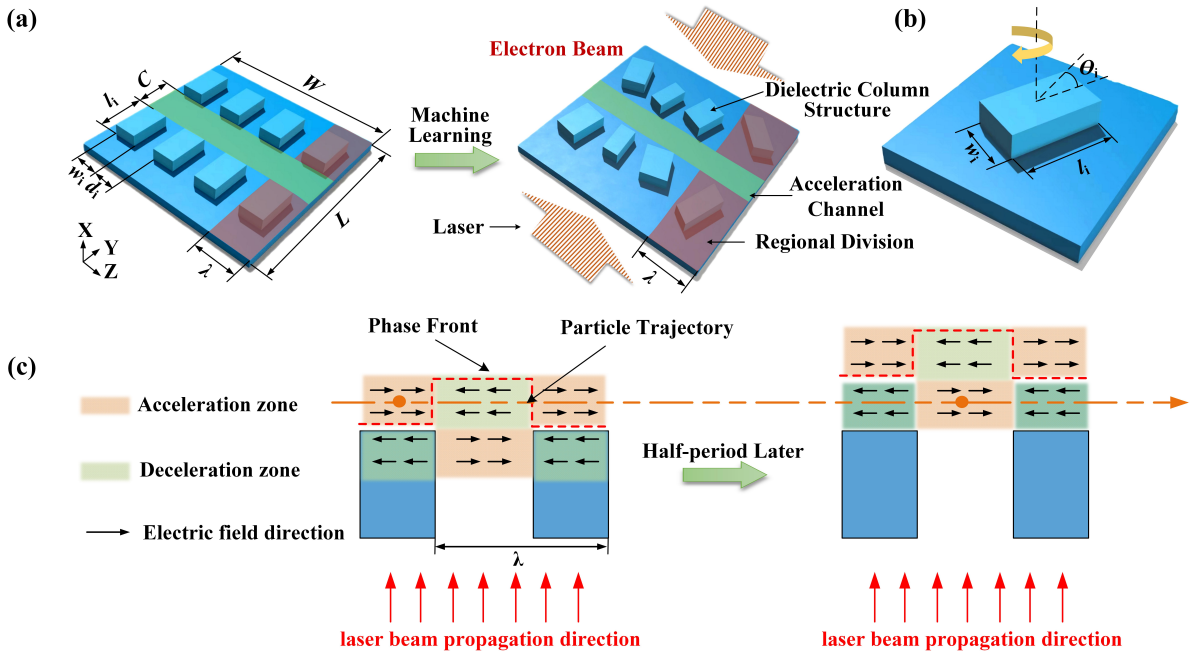


Fig. 1: Design scheme of the dielectric grating accelerator and its principle of sustained acceleration. (a) Design scheme of the dielectric grating accelerator. (b) Structural design and relevant parameters. (c) Principle of sustained acceleration in the dielectric grating accelerator.

- Length  $l_i$  varies from  $0.7 \mu\text{m}$  to  $1.5 \mu\text{m}$  in  $0.1 \mu\text{m}$  intervals;
- Width  $w_i$  ranges from  $0.4 \mu\text{m}$  to  $1 \mu\text{m}$  in  $0.1 \mu\text{m}$  increments;
- Rotation angle  $\theta_i$  varies from  $-8^\circ$  to  $8^\circ$  in  $1^\circ$  steps.

The structure is divided into four modules, with a total of twelve sets of geometric feature parameters. Additional parameters, such as optical intensity, particle injection energy, and incidence angles, were taken into account in the analysis. Numerical simulations were performed using commercial electromagnetic finite element analysis software. Furthermore, the dielectric pillar structures incorporate three materials:  $\text{SiO}_2$ ,  $\text{Al}_2\text{O}_3$ , and  $\text{Y}_2\text{O}_3$ , with the optimal structural parameters for each material determined concurrently, referencing the refractive indices from [23].

The second step involves inputting the acquired data into the constructed deep learning model to establish the correspondence between dielectric pillar design parameters, optical field intensity, particle injection energy, incidence angles, and particle energy gain. The model's reliability is evaluated; upon validation, the test dataset is fed into the trained model to predict the particle energy gain associated with each parameter set. The optimal structural parameters corresponding to the maximum particle energy gain are selected for the accelerator structure optimization. Figure 2(b) presents the proposed acceleration gradient prediction model, which achieves precise predictions through a complex network ensemble.

The GANDALF model, designed for deep feature learning, consists of two main components [35]: the Gated Fea-

ture Learning Unit (GFLU) and a Multilayer Perceptron (MLP). These components optimize tabular data performance through hierarchical feature learning and selection. The GFLU serves as the core module of the GANDALF model, adapted from the design of Gated Recurrent Units (GRUs) for non-sequential tabular data. Each GFLU stage utilizes learnable feature masks ( $M_n$ ) to select important features, generated through sparse transformations that employ the t-SoftMax function, efficiently achieving sparsity while minimizing computational overhead. The GFLU includes reset ( $r_n$ ) and update gates ( $z_n$ ), which determine how much information is discarded from the previous hidden state and the extent of updates to the current feature representation, respectively. Specifically, the reset gate dictates the amount of prior information to discard, while the update gate establishes the weight of the current candidate feature representation in the final output. This dynamic adjustment of feature selection and representation learning is facilitated by the unique weight matrices in each GFLU layer, allowing different layers to focus on different feature subsets throughout the learning process. This hierarchical structure progressively optimizes feature representation, thereby enhancing model performance. GFLU layers can be sequentially stacked to form a more robust feature representation learning network. Following the GFLU modules, the feature representations are passed to a standard MLP. In GANDALF, the MLP serves as the final prediction layer for processing the feature representations.

The feature representations obtained after multiple GFLU stages ( $H$ ) are input into a standard  $K$ -layer MLP, which maps the GFLU-optimized features to the final output di-

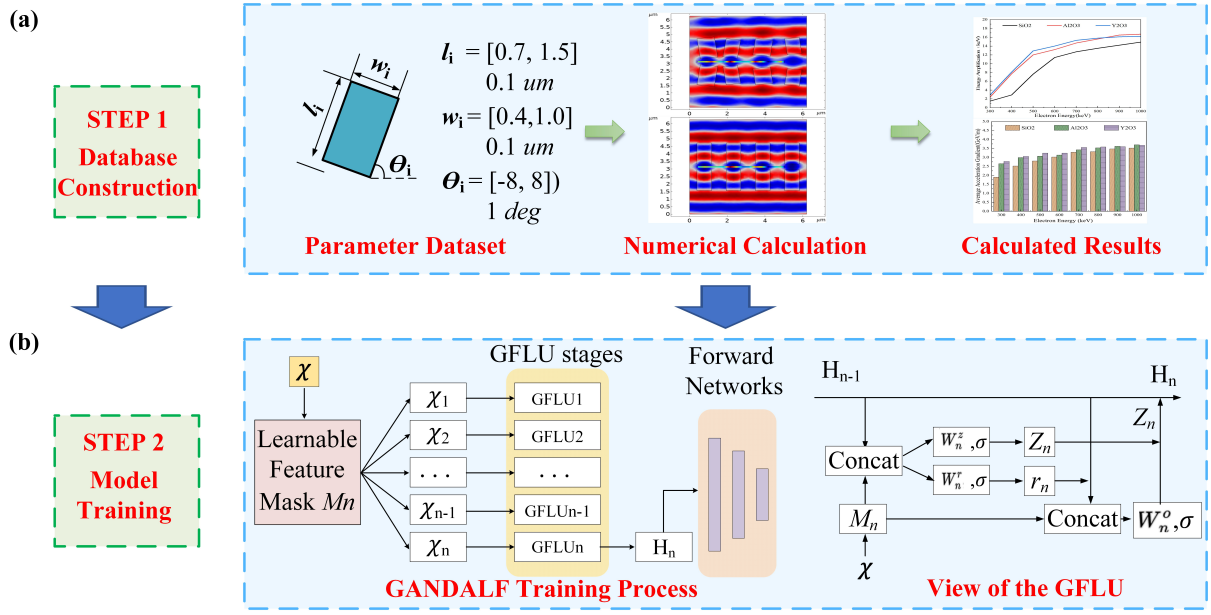


Fig. 2: Schematic of the GANDALF model. (a) Data sources and database construction. (b) Construction and internal structure of the GANDALF model.

mensions. To evaluate the GANDALF-based deep learning model, the Mean Squared Error (MSE) and the Coefficient of Determination  $R^2$  are adapted, with MSE employed as the loss function. The model optimizer employed is the Adam optimizer.

### III. RESULTS AND DISCUSSION

#### A. Performance Evaluation of the GANDALF Model

The deep learning framework proposed in this study demonstrates strong predictive capability, accurately forecasting the particle energy gain of the DLA under complex parameters. Additionally, the GANDALF model effectively selects parameters from complex information and establishes a valid relationship between its inputs and outputs, enabling the design of complex grating accelerators with nonperiodic structural configurations. The dataset for the model uses the geometric parameters of the dielectric pillars  $\mathbf{D}_i$  as inputs and the particle energy gain as the output. To ensure the reliability of the model, the dataset is randomly divided into training, test, and validation sets in a ratio of 7:2:1. Figure 3(a) presents the kernel density estimation (KDE) plots for the training, test, and validation sets within the deep learning dataset, reflecting the consistency of the dataset. The KDE distributions for the three datasets range from 0.12 to 0.16, with minimal numerical differences, indicating that the distributions of the training, test, and validation sets adequately represent the statistical characteristics of the particle acceleration gradient well. A Pearson correlation analysis of the twelve feature parameters of the dielectric pillars (Figure 3(b)) reveals that all correlation coefficients are below 0.3, indicating that the feature parameters are relatively indepen-

dent and exhibit no significant correlation, which confirms that the dataset used by the model has statistical reliability.

The GANDALF model was trained using the acquired dataset, and to further assess its predictive performance, 30 sample data points were randomly selected for testing. The test results are illustrated in Figure 4(a), where the  $R^2$  values for the three datasets are 0.942, 0.946, and 0.932, respectively. Figure 4(b) depicts the relationship between the actual and predicted values, providing a comprehensive evaluation of the model's accuracy. The model's loss function, shown in Figure 4(c), indicates that as the number of epochs increases, the loss values for both the training and validation sets remain consistently below 0.03 and converge. The GANDALF-based deep learning model demonstrates strong performance in this predictive task. The hyperparameter settings for the GANDALF model are detailed in Table 1. These results collectively indicate that the model can accurately predict particle energy gain, with predicted and actual values exhibiting a high degree of overlap and good alignment, thereby confirming the GANDALF model's high stability and robustness.

Table 1: Hyperparameter Settings for the GANDALF Model.

Hyperparameter	Value
num_GFLUs	6
num_trees	50
tree_depth	6
lr	0.001
num_epochs	30



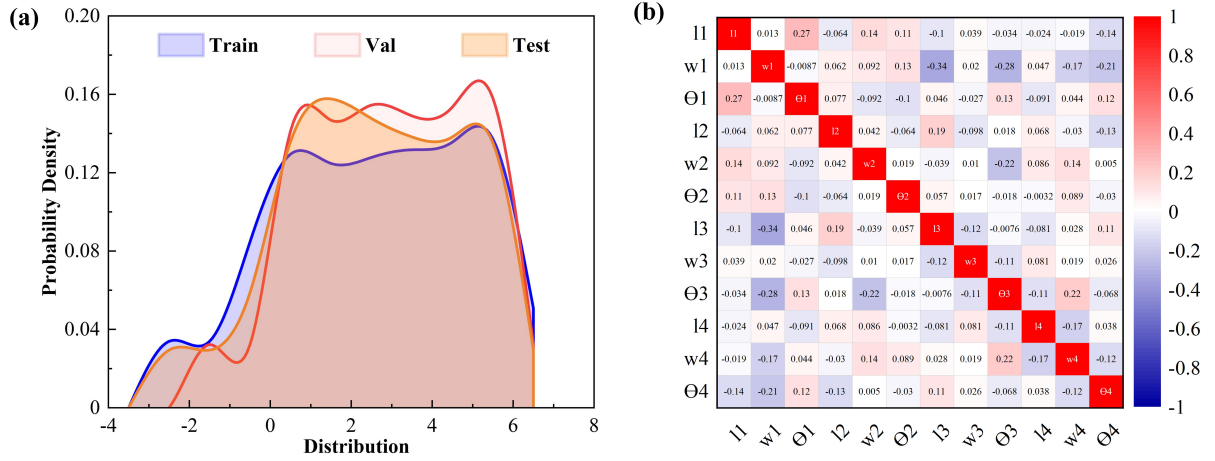


Fig. 3: Dataset distribution and parameter correlation analysis. (a) Distribution of data sets. (b) Parameter correlation analysis.

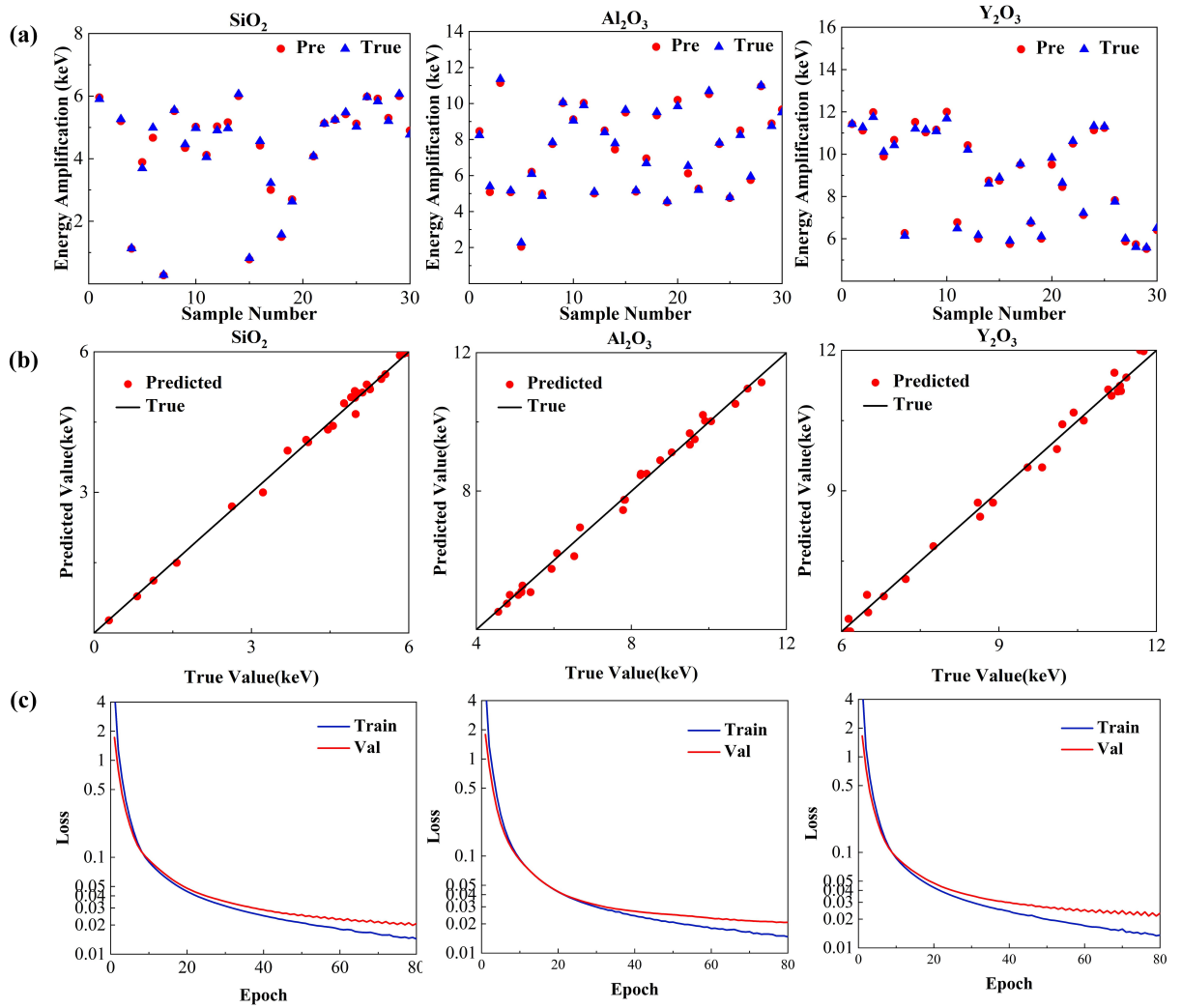


Fig. 4: Prediction results and model performance evaluation. (a) Prediction results. (b) Model performance. (c) MSE curves for the test set and training set.

### B. Optimization and Evaluation of Dielectric Grating Accelerator Structure

Upon validating the reliability of the model, the structural parameters were input into the fully trained deep learning model. This process predicted the particle energy gain corresponding to each set of parameters. The model structure parameters corresponding to the maximum particle acceleration gradient were selected. These parameters were adopted as the optimal parameters for the grating structure model of this study, facilitating structural optimization of the accelerator.

To further demonstrate the superior performance of the dielectric grating accelerator designed in this work, a periodic grating structure was introduced as a benchmark for comparison. This structure was designed using traditional optimization methods. The evaluation of sustained acceleration was conducted by comparing the first derivative of particle energy gain between the two models. A controlled variable method was employed to minimize the influence of extraneous variables. Both the periodic grating accelerator model and the one designed in this study utilized the same dielectric material. Given the broad distribution range of the model parameters designed in this study, three periodic grating structure models were constructed based on a gradient of structural parameters. The internal parameters were selected as  $w_i = d_i = \frac{\lambda_0}{2}$ , where  $\lambda_0$  represents the wavelength of the laser driving the accelerating electric field. The X-component of the particle acceleration gradient (where X denotes the direction of particle acceleration) is periodically distributed with a phase difference of  $\pi$  across neighboring regions (the  $w_i$  and  $d_i$  regions within the channel). Additionally,  $l_i$ , a crucial parameter for phase modulation within the structure, can be estimated using the following formula for the optimal periodic symmetric grating structure:

$$V_v t_0 = l_i + \frac{\lambda_0}{2} \quad (1)$$

$$V_d t_0 = l_i \quad (2)$$

Here,  $V_v$  and  $V_d$  denote the group velocities of electromagnetic waves propagating in vacuum and within the dielectric pillar, respectively. The term  $t_0$  represents the propagation time of the pulse within the dielectric pillar of length  $l_i$ . The relationship  $\frac{V_d}{V_v} = \frac{1}{n}$  holds, where  $n$  is the refractive index of the dielectric material.

$$L = \frac{\lambda_0}{2(n-1)} \quad (3)$$

For instance, taking SiO<sub>2</sub> as the dielectric material (with  $n = 1.4440$ ), the formula yields  $l_i = 1.12\lambda_0$ . Considering the impact of the particle acceleration channel width on the difficulty of particle injection and the average acceleration gradient,  $C = 0.3\lambda_0$  was selected. The corresponding particle energy gain for this structure was computed, as shown in Figure 5. This resulted in a particle acceleration gradient

of  $0.22E_0$ . The computed results indicate that the average particle acceleration gradient of the grating structure selected through the GANDALF model training reached an impressive  $0.34E_0$  (Peak electric field amplitude applied to the system at  $t = 0$ ). The particle energy gain of 8.56 keV represents 155.6% of the energy gain achieved by traditional designs, successfully meeting the anticipated experimental requirements. Detailed parameters and comparisons are provided in the supplementary materials.

In this study, the GANDALF model achieves efficient energy conversion of particles by adjusting the design parameters of the dielectric grating. Notably, the high-performance acceleration results in a more concentrated particle beam. This focused beam increases the energy density of the particle beam, enabling more efficient acceleration and more precise particle control. This characteristic is of significant importance in a wide range of high-energy physics experiments and material processing applications. The effects of different refractive index materials (SiO<sub>2</sub>, Al<sub>2</sub>O<sub>3</sub>, Y<sub>2</sub>O<sub>3</sub>) on particle acceleration performance are compared, as shown in Figure 6(a). The model provides optimized structures that are tailored to different materials. Y<sub>2</sub>O<sub>3</sub>, in contrast to SiO<sub>2</sub>, possesses better light confinement properties due to its higher refractive index. Additionally, the influence of the initial energy of the externally injected electron beam on the average acceleration gradient was investigated. By comparing the acceleration results under three different material combinations, it is demonstrated that the dielectric grating accelerator composed of high refractive index materials achieves a higher average acceleration gradient compared to structures composed of low refractive index materials. On one hand, according to Snell's law, when a laser beam enters a high refractive index material, the refraction angle increases, allowing the beam to focus into a smaller spot. This increases the energy density of the beam in the laser acceleration region, thereby enhancing the strength of the accelerating electric field. On the other hand, in high refractive index materials, the propagation speed of the beam is reduced, causing it to focus in a smaller region. This means that the spatial distribution of the beam in the acceleration region becomes more concentrated, reducing diffraction-induced spreading and facilitating the formation of an effective standing wave acceleration field. Figure 6(c) shows the particle beam spot radius of the dielectric grating accelerators selected through the GANDALF model for the various materials. All three configurations produced high-energy particle beams characterized by a beam spot radius of  $3.13 \mu\text{m}$  and a transmission efficiency of 100%. This indicates that the particle beams maintain high transverse focusing and spatial confinement throughout the acceleration process. A smaller beam spot radius indicates a more concentrated spatial distribution of the particle beam, thereby enhancing the energy density. This high energy density is conducive to achieving greater precision and efficiency in particle acceleration and material processing. Moreover, a smaller beam spot radius implies a reduced beam divergence. This enhances the stability and accuracy of particle beams during long-distance transmission. Such stability is crucial for implementing long-distance cascaded designs, particularly in

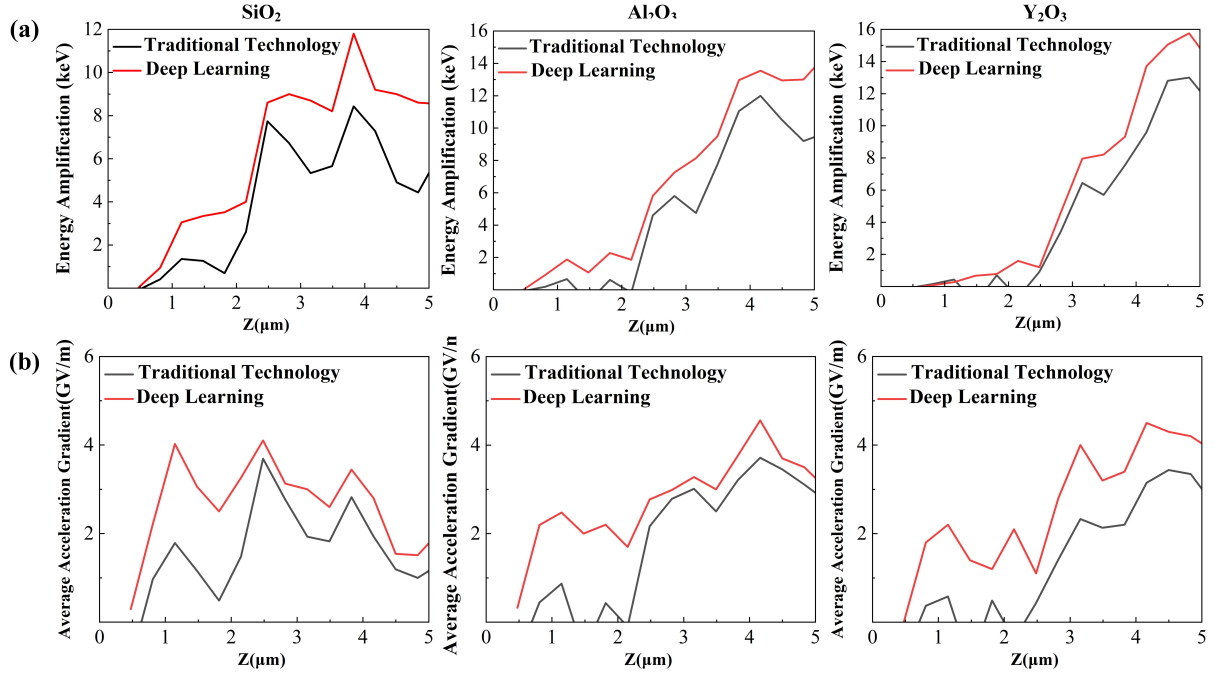


Fig. 5: Optimization results and performance evaluation of dielectric grating accelerators using SiO<sub>2</sub>, Al<sub>2</sub>O<sub>3</sub> and Y<sub>2</sub>O<sub>3</sub>. (a) Comparison of particle energy gain between traditional designs and deep learning designs for the grating structure. (b) Comparison of acceleration gradient between traditional designs and deep learning designs for the grating structure.

applications requiring long-distance, high-precision acceleration, such as high-energy physics experiments and advanced materials science research. Furthermore, the grating structure has a size of approximately 6 μm. This size is commensurate with the particle beam spot radius, effectively optimizing the grating operating conditions. The coordinated design of the grating size and beam spot radius not only enhances acceleration efficiency but also mitigates non-ideal effects such as beam spreading and diffraction distortion that may arise during grating operation. This design optimization ensures that the particle beam maintains optimal acceleration conditions and minimal optical losses while traversing the grating.

### C. Cascaded Design

The GANDALF framework supports the design of acceleration structures over extended distances, contingent upon available computational resources. However, the computational workload of the model increases substantially with the number of units and the total acceleration distance. To further enhance the net gain of particle energy, a conceptual framework for cascade acceleration design is proposed. The schematic illustration of this approach is depicted in Figure 7. As illustrated, the cascade accelerator is conceptualized as two unit cell structures. The initial injected particle energy is 500 keV. By applying the optimization scheme proposed in this study to the first unit cell structure, a net energy gain of 15.8 keV is achieved. Subsequently, the particles exiting the first unit cell structure are injected into the second unit cell structure, which is similarly optimized. This results in a cumulative net energy gain of 29.7 keV. This outcome validates the cascade accelerator design concept proposed in this study.

In cascaded dielectric laser accelerators, electron beam velocity matching requires dynamic adaptation to energy evolution. As electrons transition from the non-relativistic ( $\beta < 0.5$ ) to the relativistic regime ( $\beta \rightarrow 1$ ), the pulse front tilt (PFT) angle must satisfy:

$$\theta_{\text{PFT}}(z) = \arcsin(\beta(z)) \quad (4)$$

This relationship dictates continuous adjustment of  $\theta_{\text{PFT}}$  along the propagation distance  $z$  under fixed acceleration gradients. To achieve dynamic matching, a DMD-LCM (Digital Micromirror Device-Liquid Crystal Mask) coordination and regulation strategy is proposed:

1. **Spatiotemporal Encoding:** Preloaded phase-amplitude masks (corresponding to  $\beta$ -dependent  $\theta_{\text{PFT}}$  requirements) are dynamically addressed on the DMD, with spatial encoding converted to temporal modulation via PFT techniques.
2. **Adaptive Switching:** When electrons enter the  $n$ th acceleration stage, the LCM activates the corresponding mask based on real-time beam parameters (feedback from upstream diagnostics).
3. **Timing Performance:** With commercial DMDs (e.g., DLP9500) exhibiting 20 μs switching times and LCMs demonstrating millisecond-scale responses, parallel control strategies reduce system latency to  $\sim 50$  μs, which is compatible with standard electron gun repetition rates (typically  $\leq 1$  kHz).

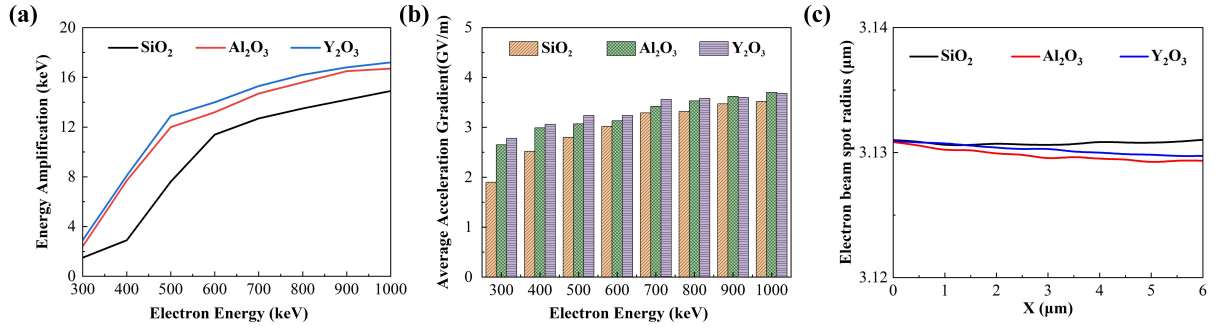


Fig. 6: Performance evaluation and particle dynamics of optimized DLA grating structures for SiO<sub>2</sub>, Al<sub>2</sub>O<sub>3</sub> and Y<sub>2</sub>O<sub>3</sub> using deep learning. (a) Energy gain as a function of initial injection energy. (b) Average acceleration gradient as a function of initial injection energy. (c) Beam spot radius as a function of transverse displacement in the acceleration channel.

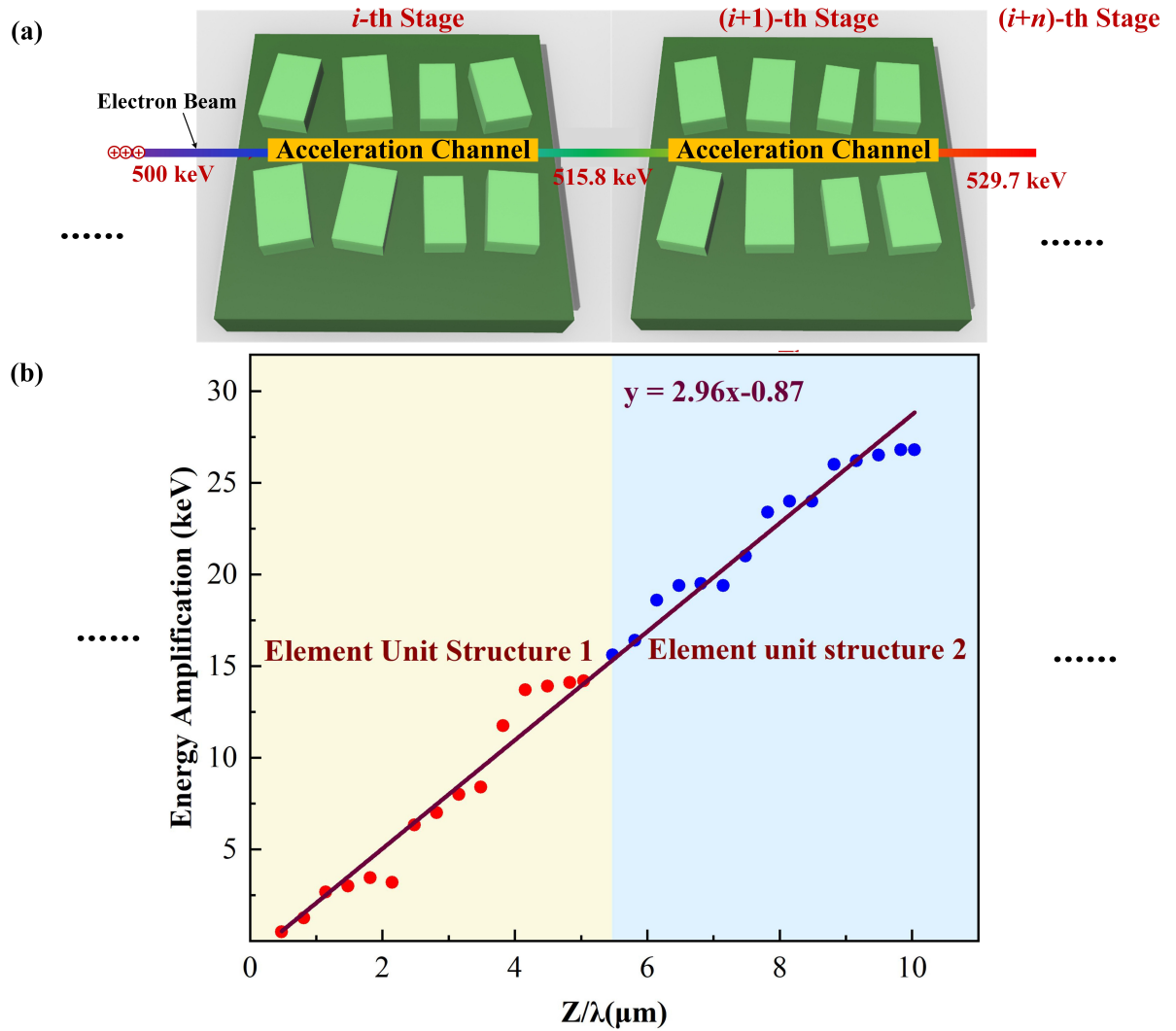


Fig. 7: Schematic of the cascaded grating accelerator and its acceleration performance. (a) Schematic of the cascaded grating accelerator. (b) Impact of different unit cell structures on particle energy gain.

This approach enables continuous adjustment of  $\theta_{\text{PFT}}$  from 17° to 45° (corresponding to  $\beta = 0.3\text{--}0.99$ ), outperforming

fixed-angle solutions optimized for the extreme relativistic regime ( $\beta \approx 1$ ). Theoretical analysis confirms that angu-



lar deviations  $\Delta\theta < 0.5^\circ$  maintain phase slippage  $\Delta\phi$  below  $\lambda/30$  ( $\lambda = 2\ \mu\text{m}$ ), effectively suppressing transverse emittance growth due to velocity mismatch. Building on the inherent compatibility between PFT techniques and spatial light modulators[36], this method provides a modular implementation pathway for cascaded accelerators. Future work will focus on developing closed-loop control systems integrating real-time beam position monitoring and mask optimization algorithms to improve matching precision.

#### IV. CONCLUSION

This work proposes a novel design methodology for dielectric grating accelerators based on deep learning methods. By integrating deep learning with grating structure optimization, a high-performance accelerator structure and cascading design scheme are achieved. The proposed method predicts the target particle energy gain using comprehensive feature evaluation, with both training and validation losses below 0.03. The Pearson correlation coefficient was employed to assess the validity of the database, revealing that the feature parameters are relatively independent with no significant cor-

relations. The optimal particle energy gain was then predicted, and the corresponding structural parameters were selected as the optimal model parameters, enabling the optimization of the dielectric grating accelerator structure. A comparison between the dielectric laser accelerator designed in this study and those designed using traditional methods demonstrated that the  $\text{SiO}_2$  grating accelerator designed here achieves a particle energy gain of 130.3% relative to the periodic structure. The  $\text{Y}_2\text{O}_3$  grating accelerator designed in this study achieved a maximum average acceleration gradient of 2.8 GV/m ( $\text{Y}_2\text{O}_3$ ). The post-acceleration particle beam transmission efficiency is 100%, with a beam spot radius of 3.13  $\mu\text{m}$ , providing data support for cascaded accelerator designs. This research offers valuable insights for the design of particle accelerators based on photonic chips and the integration of optoelectronic devices. Moreover, it introduces a novel design approach for nonperiodic photonic crystals and complex sub-wavelength optoelectronic devices.

##### A. Data Availability

Data underlying the results presented in this paper are not publicly available at this time but can be obtained from the authors upon reasonable request

##### B. Disclosures

The authors declare no conflicts of interest.

#### V. REFERENCES

- [1] W. Yao, M. Nakatsutsumi, S. Buffechoux, et al., "Optimizing laser coupling, matter heating, and particle acceleration from solids using multiplexed ultraintense lasers," *Matter Radiat. Extremes* **9**, 047202 (2024). doi:10.1063/5.0184919
- [2] J. R. Marquès, L. Lancia, P. Loiseau, et al., "Collisionless shock acceleration of protons in a plasma slab produced in a gas jet by the collision of two laser-driven hydrodynamic shockwaves," *Matter Radiat. Extremes* **9**, 024001 (2024). doi:10.1063/5.0178253
- [3] Y. Zhang, W. C. Fang, X. X. Huang, et al., "Design, fabrication, and cold test of an S-band high-gradient accelerating structure for compact proton therapy facility," *Nucl. Sci. Tech.* **32**, 38 (2021). doi:10.1007/s41365-021-00869-z
- [4] S. G. Tantawi, V. Dolgashev, Y. Higashi, et al., "Research and development for ultrahigh gradient accelerator structures," in *Advanced Accelerator Concepts: 14th Advanced Accelerator Concepts Workshop*, AIP Publishing, 2010, vol. 1299, pp. 29–37. doi:10.1063/1.3520332
- [5] E. A. Peralta, K. Soong, R. J. E., et al., "Demonstration of electron acceleration in a laser-driven dielectric microstructure," *Nat.* **503**, 91–94 (2013). doi:10.1038/nature12664
- [6] R. L. Byer, E. A. Peralta, S. Tsujino, et al., "Dielectric laser accelerators," *Rev. Mod. Phys.* **86**, 1337–1385 (2014). doi:10.1103/RevModPhys.86.1337
- [7] K. Mizuno, S. Ono, O. Shimoe, "Experimental evidence of the inverse Smith–Purcell effect," *Nat.* **253**, 184 (1987). doi:10.1038/328045a0
- [8] K. Soong, R. L. Byer, E. R. Colby, et al., "Laser damage threshold measurements of optical materials for direct laser accelerators," *AIP Conf. Proceed.* **1507**, 511 (2012). doi:10.1063/1.4773749
- [9] R. Agustsson, E. Arab, A. Murokh, et al., "Measuring single-shot, picosecond optical damage threshold in Ge, Si, and sapphire with a 5.1- $\mu\text{m}$  laser," *Opt. Mater. Express* **5**, 2835–2842 (2015). doi:10.1364/OME.5.002835
- [10] D. Cesar, J. Maxson, P. Musumeci, et al., "Optical design for increased interaction length in a high gradient dielectric laser accelerator," *Nucl. Instrum. Methods A* **909**, 252–256 (2018). doi:10.1016/j.nima.2018.01.012
- [11] J. Breuer, J. McNeur, P. Hommelhoff, "Dielectric laser acceleration of electrons in the vicinity of single and double grating structures—Theory and simulations," *J. Phys. B At. Mol. Opt. Phys.* **47**, 234004 (2014). doi:10.1088/0953-4075/47/23/234004
- [12] T. Plettner, R. L. Byer, B. Montazeri, "Electromagnetic forces in the vacuum region of laser-driven layered grating structures," *J. Mod. Opt.* **58**, 1518 (2011). doi:10.1080/09500340.2011.611914
- [13] D. S. Black, Z. X. Zhao, K. J. Leedle, et al., "Operating modes of dual-grating dielectric laser accelerators," *Phys. Rev. Accel. Beams* **23**, 114001 (2020). doi:10.1103/PhysRevAccelBeams.23.114001
- [14] D. Cesar, S. Custodio, J. Maxson, et al., "High-field nonlinear optical response and phase control in a dielectric laser accelerator," *Commun. Phys.* **1**, 46 (2018). doi:10.1038/s42005-018-0047-y
- [15] X. E. Lin, "Photonic band gap fiber accelerator," *Phys. Rev. Spec. Top. Accel. Beams* **4**, 051301 (2001). doi:10.1103/PhysRevSTAB.4.051301
- [16] B. M. Cowan, "Three-dimensional dielectric photonic crystal structures for laser-driven acceleration," *Phys. Rev. Spec. Top. Accel. Beams* **11**, 011301 (2008).

- doi:10.48550/arXiv.0711.3190
- [17] X. Mei, R. Zha, Y. Pan, et al., “Dielectric laser accelerators driven by ultrashort, ultraintense long-wave infrared lasers,” *Ultrafast Sci.* **3**, 0050 (2023). doi:10.34133/ultrafastscience.0050
  - [18] T. Plettner, R. L. Byer, B. Montazeri, “Electromagnetic forces in the vacuum region of laser-driven layered grating structures,” *J. Mod. Opt.* **58**, 1518–1528 (2011). doi:10.1103/PhysRevSTAB.12.101302
  - [19] L. Brückner, T. Chlouba, Y. Morimoto, et al., “Mid-Infrared Dielectric Laser Acceleration in a Silicon Dual Pillar Structure,” *Opt. Express* **32**, 28348 (2024). doi:10.1364/OE.531071
  - [20] N. V. Sapra, K. Y. Yang, D. Verduyn, et al., “On-chip integrated laser-driven particle accelerator,” *Sci.* **367**(6473), 79–83 (2020). doi:10.1126/science.aay5734
  - [21] T. Hughes, G. Veronis, K. P. Wootton, et al., “Method for computationally efficient design of dielectric laser accelerator structures,” *Opt. Express* **25**, 15414–15427 (2017). doi:10.1364/OE.25.015414
  - [22] R. D. Shannon, R. C. Shannon, O. M., et al., “Refractive index and dispersion of fluorides and oxides,” *J. Phys. Chem. Ref. Data* **31**, 931–970 (2002). doi:10.1063/1.1497384
  - [23] Y. F. He, B. Sun, M. J. Ma, et al., “Topology optimization of on-chip integrated laser-driven particle accelerator,” *Nucl. Sci. Technol.* **33**, 120 (2022). doi:10.1007/s41365-022-01101-2
  - [24] W. Ma, Y. Xu, B. Xiong, et al., “Pushing the limits of functionality—Multiplexing capability in metasurface design based on statistical machine learning,” *Adv. Mater.* **34**, 2110022 (2022). doi:10.1002/adma.202110022
  - [25] X. Liu, P. Wang, C. Xiao, T. Fan, et al., “Compatible stealth metasurface for laser and infrared with radiative thermal engineering enabled by machine learning,” *Adv. Funct. Mater.* **33**, 2212068 (2023). doi:10.1002/adfm.202212068
  - [26] Q. Zhang, C. Liu, X. Wan, et al., “Machine-learning designs of anisotropic digital coding metasurfaces,” *Adv. Theory Simul.* **2**, 1800132 (2019). doi:10.1002/adts.201800132
  - [27] C. Wang, X. Cheng, R. Wang, et al., “Flexibly designable 2D chiral metasurfaces with pixelated topological structure based on machine learning,” *Laser Photonics Rev.* **18**, 2300958 (2024). doi:10.1002/lpor.202300958
  - [28] K. Pachori, A. Prakash, N. Kumar, “Effective modeling of metasurface-loaded circularly polarized dielectric resonator-based MIMO antenna for sub-6.0-GHz band using machine learning algorithms,” *Int. J. Commun. Syst.* **37**, e5738 (2024). doi:10.1002/dac.5738
  - [29] Z. D. Lei, Y. D. Xu, D. Wang, et al., “Dynamic multifunctional metasurfaces: an inverse design deep learning approach,” *Photon. Res.* **12**, 123–133 (2024). doi:10.1364/PRJ.505991
  - [30] B. Hermann, U. Haeusler, G. Yadav, et al., “Inverse-Designed Narrowband THz Radiator for Ultrarelativistic Electrons,” *ACS Photonics* **9**(4), (2022). doi:10.1021/acsphotonics.1c01932
  - [31] L. Bruckner, T. Chlouba, R. Shiloh, et al., “Coherent Particle Acceleration on a Nanophotonic Chip,” in *2024 37th International Vacuum Nanoelectronics Conference (IVNC)*, Brno, Czech Republic, 2024, pp. 1–2. doi:10.1364/FIO.2023.FW6C.3
  - [32] T. W. Hughes, S. Tan, Z. X. Zhao, et al., “On-chip laser-power delivery system for dielectric laser accelerators,” *Phys. Rev. Appl.* **9**, 054017 (2018). doi:10.1103/PhysRevApplied.9.054017